A Novel Visualization Enabled Decision Support Framework for Data-Driven Integrated Design Space Exploration

Rashmi Rama Sushil[1a], Mathew Baby[2a], Gehendra Sharma[3], Anand Balu Nellippallil[2b], Palaniappan Ramu[1*]

[1a]Graduate student, Advanced Design, Optimization, and Probabilistic Techniques Laboratory, Indian Institute of Technology Madras, Chennai, 600036, Tamil Nadu, India.
[2a]Graduate student, Systems Realization Laboratory, Florida Institute of Technology, Melbourne, 32901, Florida, USA.
[3]Research engineer, Center for Advanced Vehicular Systems, Mississippi State University, Starkville, 39759, Mississippi, USA.
[2b]Assistant Professor, Systems Realization Laboratory, Florida Institute of Technology, Melbourne, 32901, Florida, USA.
[1*]Associate Professor, 314, Department of Engineering Design, Indian Institute of Technology Madras, Chennai, 600036, Tamil Nadu, India.

*Corresponding author(s). E-mail(s): palramu@iitm.ac.in;
Contributing authors: rashmi.ramasushil@gmail.com[1a];
mbaby2021@my.fit.edu[2a]; gs1092@cavs.msstate.edu[3];
anellippallil@fit.edu[2b];

A Novel Visualization Enabled Decision Support Framework for Data-Driven Integrated Design Space Exploration

Abstract

Design preferences or targets are typically available at the system level. A designer is usually interested in understanding patches of the design space at component levels, across different stages and processes that correspond to such system targets or preferences. This demands a thorough design space exploration permitting both forward and inverse designs. Such exploration becomes cumbersome with a large number of variables and complex systems with many conflicting goals. Hence a decision support framework that permits seamless navigation in high dimensions, especially with a visual aspect for enhanced comprehension, is desirable. Current work proposes using a data-driven interpretable self organising map (iSOM) as a visual enabler in decision support systems for exploring the design space and understanding the trade-off in system goals. The novelty lies in being able to use a visual form to compare greater than three conflicting goals simultaneously while accounting for design variables. The proposed approach is demonstrated using two test problems: i) hot rolling and cooling process chain design for the production of steel rods, and ii) head and neck-injury risk evaluations for vehicular crash-worthiness. Using the first problem, we demonstrate the capability of iSOM to support the solution space exploration of a many-goal steel manufacturing process chain problem to realize the design of a steel product, in the context of a compromise Decision Support Problem formulation. In the second problem, we demonstrate the capability of iSOM to support early-stage Design Space Exploration (DSE) to identify critical injury-risk regions of interest for different car crash scenarios. These two test problems illustrate the capability to carry out a forward and inverse design, by the proposed approach.

Keywords: Design Space Exploration, Interpretable Self Organizing Maps, Compromise Decision Support Problems

1 Introduction

The design of complex systems such as automobiles, aircraft, and ships requires multidisciplinary knowledge and expertise [1]. Such systems are characterized by the presence of many design variables, constraints, and goals across multiple disciplines,

and their complex interactions. Hence, during such design, designers 'make decisions' that meet multiple conflicting goals while simultaneously accounting for the constraints. In the early stages of the design of complex multidisciplinary systems, designers often have a limited understanding of the complex interactions and their influence on the design spaces of the system. Given the limited understanding, the designer's interest lies in quickly identifying a ranged set of design solutions that meet their requirements, and not in identifying unique single-point solutions. The identification of a ranged set of solutions that meet the designer's requirements is facilitated by carrying out design space exploration (DSE). To effectively carry out DSE for complex systems, designers require an understanding of the complex system in terms of the trade-off between many conflicting goals, and the relations between the design variables and system responses. The use of visualization techniques helps enhance the designer's understanding of the complex system by supporting the visualization of the trade-offs between conflicting goals and the complex relations between the variables and goals in the system. Therefore, by performing DSE assisted by visualization techniques, designers are able to make informed design decisions in identifying a ranged set of design solutions that meet their requirements.

The visualization of the design spaces of complex systems is challenging, given the large dimensions of the design spaces that arise from the many variables and goals involved. Different techniques are discussed in the literature to support the visualization of the design spaces of complex systems. In the past, researchers have used dimension reduction techniques to deal with large dimensions [2] and used techniques such as parallel coordinates plots, nested axis plots, ternary plots, and t-Stochastic Neighbour Embedding (t-SNE), among others, for visualization. These visualization techniques developed in the past are useful [3] but are usually limited to comparing three or four parameters ([4, 5]) at a time. The parameters could be input variables or output responses. A detailed comparison of such techniques is provided in [6].

Previous attempts at supporting DSE for complex engineered systems, using multi-dimensional visualization techniques [7] lack the capability to visualize design/solution spaces simultaneously with all objectives ([8, 9]). In [10], the solution space is explored using ternary plots, which enable navigation in 3 dimensions/goals. [11] uses scatter plots and parallel coordinate plots for visualizing multiple objectives and attributes, respectively. As the dimensions increase, the plots are difficult to interpret, computationally demanding, and in some cases, not able to capture the information correctly in reduced dimensions as well [12]. Owning to the above limitations in the existing visualization techniques ([13, 14]), it is desirable to develop visualization techniques that permit DSE with limited computation and are inherently interpretable so that one can address DSE of complex systems characterized by a large number of goals, constraints, variables, and their complex interactions. The importance of enhancing visualization techniques has been further heightened due to the availability of intricate and high-dimensional data, which is used in studying complex phenomena in different fields of research [15].

To support the design of complex systems, multidisciplinary optimization (MDO) techniques are proposed ([16–19]). Some examples include analytical target cascading

(ATC) [20], collaborative optimization (CO) [21], and bilevel integrated system synthesis (BLISS) [22]. These MDO approaches generally employ rigorous optimization techniques to identify 'point solutions' at each discipline and usually involve a substantial number of iterations within and between disciplines using optimization loops until convergence is achieved. This is particularly challenging in early-stage design exploration, where the focus is on quickly identifying satisfactory design spaces (regions or sets) instead of a unique single-point solution [23]. An alternative to optimization and optimization-based techniques is the 'satisficing' philosophy that is anchored in the notion of 'bounded rationality' proposed by Herbert A. Simon [24]. In the 'satisficing school of thought,' the designer's focus is not on meeting the requirements in the best possible manner but rather on meeting acceptability thresholds for the requirements by exploring the available alternatives and identifying a 'ranged set of satisficing solutions'.

A satisficing solution [25] is a solution that 'satisfy' and 'suffice' the designer's requirements for the conflicting goals present. Mistree and co-authors [26] propose the Decision-Based Design (DBD) paradigm that is based on the satisficing philosophy. In DBD, design is considered a decision-making process wherein designers make a series of decisions, some sequentially while others concurrently. Muster and Mistree [27] propose the Decision Support Problem (DSP) technique to support the DBD paradigm. The DSP Technique is anchored in the notion of bounded rationality. The designer's focus when employing the DSP technique is on identifying a 'set of satisficing solutions', rather than identifying a unique single-point solution. The compromise Decision Support Problem (cDSP) [28] is a well-established DSP technique in the literature that is used to explore satisficing solutions for many conflicting goals. Inductive Design Exploration Method (IDEM) [29] and Goal-oriented Inverse Design (GoID) [10] are two DBD methods that have been discussed in the literature to support the design of complex multi-level systems. Both methods make use of the cDSP construct to identify satisficing solutions for many conflicting goals across multiple levels. The IDEM is especially suitable for hierarchical design problems and is suitable for managing the propagation of different sources of uncertainty across levels in complex multilevel systems. Using the IDEM, the designer's goal is to identify satisficing solution sets within a feasible solution space and communicate these sets across multiple levels. However, IDEM has certain limitations, as outlined in [30]. These include: i) limitations in terms of flexibility in design as IDEM does not facilitate the incorporation of new goals or requirements at different levels during the design process as the method is based on top-down mapping to feasible spaces, ii) discretization errors since IDEM discretizes the design space resulting in an inability to capture the feasible boundary accurately, iii) increased computational expense if the accuracy is increased by adding more discretized points, iv) limitation in terms of the number of design variables that can be studied (impossible beyond nine variables) thus limiting the problem size, v) limitations in exploration and visualization as only a maximum of three design variables can be studied at a time by assigning fixed values to the other variables. The GoID method is also a multilevel design method where decisions are made separately at each level (using separate cDSPs), and the output from one level, becomes the input (goals) for the preceding level in the sequence. This method addresses the limitations of IDEM

by offering improved flexibility (in terms of the capability to define new goals and requirements) as separate cDSPs are used for different levels of decision-making, and it can also handle n number of design variables (an improvement over IDEM, which is limited to nine).

In the GoID method, the designer makes use of ternary plots to visualize the solution space at each level. Using the ternary plot, the designer visualizes a continuous feasible solution space of a goal, across different design scenarios by only considering a maximum of 3 goals. Hence, the GoID approach is limited by the ability of the ternary plot to visualize a solution space. The use of ternary plots limits the designers to have a maximum of 3 goals in cDSP problem formulations, and any additional goals are required to be formulated as constraints that are hard requirements that always have to be satisfied. This limitation, when using ternary plot-based visualization to support DSE, can potentially result in the loss of some satisficing design solutions. Hence, there is a need to overcome this limitation to ensure a more thorough exploration of the design spaces during the early stages of design. This requires the use of visualization techniques that permit visualization of higher-dimensional (more than 3) design spaces.

The key focus in this paper is on presenting a visual enabler that can overcome the limitations associated with the use of ternary plot-based visualization during design/-solution space exploration to identify satisficing solution sets and, at the same time, is inherently interpretable. But comparing the ease of interpretability of different visualization techniques is not an easy task [31]. It is usually subjective, as different individuals have different preferences and abilities to interpret information presented visually. It is desirable that the plots from the visualization technique are based on simple logic and do not get cumbersome with large data or large dimensions. Several visualization techniques, such as Contour plots, Heat Maps, Scatter plots, PCP, RadViz, t-SNE, Kohonen's Self Organizing Map (SOM), and interpretable Self Organizing Map (iSOM) among others, are discussed in the literature that supports the visualization of high-dimensional design spaces. Kohonen's SOM is a class of artificial neural networks commonly used to visualize high-dimensional data in 2D planes [20]. In the recent past, SOM has been used successfully for DSE that involves visualizing tradeoffs in Pareto solutions [32], selection of data for multi-objective optimization [33], and sampling-driven design space reduction [34, 35]. [36] developed a variant of SOM named iSOM, where the outputs are inherently interpretable while avoiding self-aberration. [6] provides a comprehensive comparison of PCP, Heat maps, RadViz plots, t-SNE plots, and iSOM. iSOM has distinct advantages such as scalability and interactiveness as discussed in [6], making it the suitable choice for exploring design space in real-world problems. The utility of iSOM in aiding design space exploration of real-world problems is presented in [37] and [38]. In [37], the use of iSOM for design space exploration of a manufacturing supply network design problem is presented. In [38], the authors present the utility of the iSOM visualization in the design of a steel hot-rod rolling system involving products, materials, and manufacturing processes.

In this paper, we present a framework to help designers visualize the design space of complex systems with many goals and variables, in order to aid designers in carrying out design/solution space exploration and identifying a ranged set of satisficing

solutions for design problems formulated using the cDSP construct. We present the use of iSOM as the visualization enabler for supporting design/solution space exploration in identifying a ranged set of satisficing solutions. We demonstrate the utility of the proposed framework using a material processing problem [10] and evaluation of an occupant's neck and head injury criteria for varied inputs in a car crash context. [10] presents an inverse method to achieve the integrated design exploration of materials, products, and manufacturing processes through the vertical and horizontal integration of models. In the above work, in the cDSP for the desired end mechanical properties of the product, one of the four goals (Impact Transition Temperature, ITT) is formulated as a constraint due to the use of the ternary plots to support design/solution space exploration. Ternary plots limit the designers to visualize a maximum of 3 goals at a time. In this paper, we use iSOM to visualize all 4 goals of the material processing problem simultaneously and demonstrate the utility of iSOM in enhancing the confidence of designers in making design decisions. Using the car crash example, we showcase the utility of iSOM in aiding designers to explore the problem design space to identify the high-risk region based on five neck and head injury values determined by two input variables, namely the impact velocity and impact angle. In the process, iSOM provides the visualization of 5 injury metrics (responses) for 2 input variables.

The novelty of the work presented in this paper lies in combining iSOM with cDSP construct to support the designers in exploring the design/solution spaces of high-dimensional design problems and identifying a ranged set of satisficing solutions that meet the many (more than 3) conflicting goals, which is not possible using ternary plots. Using the examples we also demonstrate the scope of using iSOM as a decision support aid that helps designers in identifying Regions of Interest (RoI) in the design/-solution space for further exploration during i) forward design, where the focus on understanding the impact of design variables on system goals, and ii) inverse design, where the focus is on identifying the design variables that help achieve the target solutions. The proposed visualization framework for design/solution space exploration provides seamless scaling as the number of dimensions increases. In addition, comparisons such as analyzing trends or identifying correlations between variables, between goals, or between variables and goals are supported using the proposed visualization framework, as demonstrated using the test examples.

The rest of the paper is organized as follows: In Section 2, we discuss the conventional SOM implementation, followed by a discussion of the iSOM visualization employed in this work. In Section 3, we present a framework to visualize the high-dimensional design space and thereby aid designers in carrying out design/solution space exploration and identifying a ranged set of satisficing design solutions in the early-stage design of complex systems. The solution space exploration for hot rod rolling and car crash problems using iSOM-based visualization is discussed in Section 4 and Section 5, respectively, followed by concluding remarks.

2 Self Organizing Maps

Among various existing neural network architectures and learning algorithms, Kohonen's SOM is one of the most popular neural network models. Developed for an

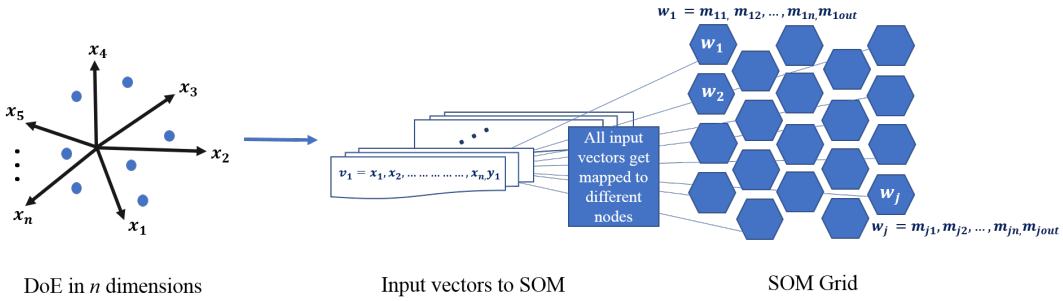

Fig. 1 Working of SOM algorithm

associative memory model, it is an unsupervised learning algorithm with a simple structure and computational form [39, 40]. It is an efficient algorithm for the visualization of multidimensional numerical data [41]. One of the important characteristics of the mapping is that it preserves topology [42] such that similar data points will be mapped to nearby locations on the map, thus conserving relative distances between input data points. This permits the user to identify the pattern in the input data.

2.1 Conventional Self Organizing Maps (cSOM)

Figure 1 presents a pictorial layout of the basic working of SOM. It consists of a mesh of nodes, arranged in a hexagonal or rectangular topology. Each input DoE sample point corresponds to an input vector in SOM. Let $v_i = [x_{i1}, x_{i2}, ..., x_{in}, y_i]$, where x_i's are input variables and y_i is the corresponding output. Each node is associated with a weight vector, $w_j = [m_{j1}, m_{j2}, ..., m_{jn}, m_{jout}]$ where the first n weights correspond to design variables and the last weight corresponds to the response. In SOM, weight vectors have the same dimension as the input data vector. Values of weights are usually initialized by linear initialization. We note the conventional implementation of SOM as cSOM to differentiate it from iSOM. In cSOM implementation, for each v_i, the node that has the minimum Euclidean distance from v_i, is selected as the best matching unit (BMU). Based on an update rule, the weight of the neighborhood nodes corresponding to the BMUs change. The BMU selection and update continue until a prescribed number of iterations or error convergence metrics are met. Trained SOM weights are obtained as the output once the iteration is over. These weights are used to construct component plane plots. In the component plane, the position of each node remains the same regardless of which attribute is being visualized, thus it helps one to visualize the weights of the selected variable, input, or output and compare it with the rest of the variables. Similar-looking component planes indicate that the corresponding variables may be correlated. Thus a trained SOM network efficiently represents how data is distributed in the design space.

Some earlier works demonstrate the use of cSOM for visualizing trade-offs and Pareto fronts in multi-objective formulations [32, 33]. Also, [43] illustrates the use of cSOM, parallel coordinate plot, and hyper radial visualization for visualization of

Pareto data related to shape optimization application. cSOM has been used to understand correlations among design variables and responses [44]. [1] proposes using cSOM on the optimization data to get an idea of the relationship between design variables and objectives to work in reduced design space. cSOM has also found applications in the area of adaptive sampling and feasible sample generation [45]. Techniques such as growing hierarchical self-organizing maps (GHSOM), a variant of cSOM are developed for visualizing Pareto optimal solutions [46]. All of the work above uses cSOM, but its implementation is known to experience aberration or self-folding, which leads to compromises in the visualization of component planes, though topology is preserved mathematically.

2.2 Interpretable Self Organizing Maps (iSOM)

In order to address the issues associated with cSOM, [36] developed iSOM, where component planes are inherently interpretable and avoid self-intersections. iSOM implementation differs from cSOM in the selection of data for BMU estimation. In iSOM, only the input data is considered as against input and output data in cSOM. In addition, the update step employs only the response value and not the input variables. These changes avoid the self-intersection or folding in iSOM. An added benefit observed is that the component plane plots obtained are in an ordered fashion permitting a simplified understanding of component planes. For further details on iSOM, the reader is referred to [36].

Plots generated using iSOM can be used to visualize the underlying correlations among variables. Figure 2 provides an overview of iSOM outcomes for a simple $z = x^2+y^2$ function. The arrows in the X and Y component planes represent the increasing direction of the axes' values. For instance, if one is interested in the region marked by the circle, in the z component plane, the corresponding x and y values are bounded by the circles placed in the x and y component planes. Such a scheme permits forward and inverse DSE. It is to be noted that the shape of the function is also preserved in the z component plane. [36] discusses how RoI can be selected based on iSOM plots irrespective of the number of dimensions. The reduced ranges of input design variables are then identified where RoI lies, allowing targeted sampling to fit a metamodel and perform optimization. The work in [47] shows that iSOM can also be used to visualize Pareto solutions for a multi-objective problem. Both these studies utilize the inherent interpretability of iSOM to explore design/solution space.

3 PROPOSED DESIGN APPROACH

Oftentimes, a designer needs to identify regions in the design space that correspond to target outputs. But the design space itself could be complex, with multiple processes and design elements. Also, mapping one target region in performance space might mean different regions across different processes or elements, which is referred to as horizontal and vertical communication as discussed in [10].The methodology introduced aims to facilitate intuitive visualization of such intricate systems for enhanced analysis.The iSOM implementation discussed here is akin to that in [6], where iSOM is trained to visualize conflicting outputs related to different input

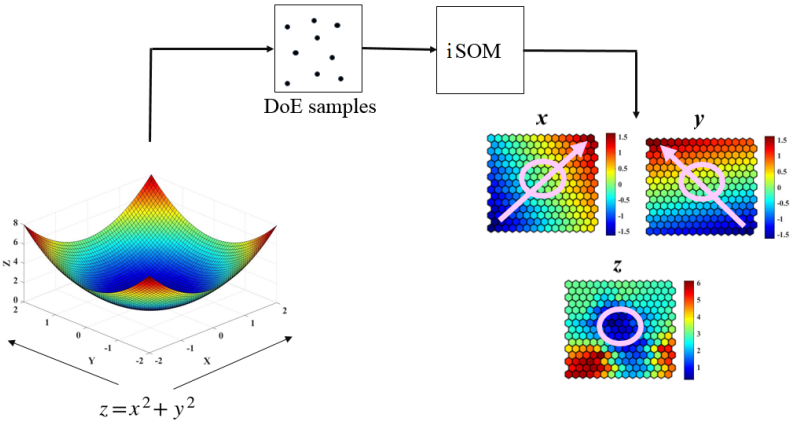

Fig. 2 An example of plots generated using iSOM for the function $z = x^2 + y^2$

variables. A key modification is in the initialization step, where a unified map grid is employed instead of separate grids for each objective function during iSOM training. The process is as follows:

Initilization: Let there be n input vectors $[a_1, a_2, ..., a_n]$, each of d dimensions: $a_i = [a_{i1}, a_{i2}, ..., a_{id}]$, i from 1 to n . Correspondingly, each input vector has m outputs, $y_i = [y_{i1}, y_{i2}, ..., y_{im}]$. To analyze the correlation of m outputs with d input dimensions, we create a common iSOM grid. Each input vector a_i is augmented with a single output g_i, which is a weighted average of all outputs: $g_i = \sum_{j=1}^{m} k_j y_{ij}$, where k_j are the weights proportional to the range of outputs respectively.

Training: Each objective function is subsequently trained independently using the unified grid established during initialization. The input vector for training is structured as: $[a_i, y_i]$.

Output: iSOM generates m output plots corresponding to n input variables. This approach allows interpretation of output plots among themselves and in relation to all input dimensions. MATLAB code [48] is modified and utilized for generating iSOM results. Figure 3 illustrates the schematic overview of the proposed design method.

We present two scenarios where designers can benefit from the proposed iSOM visualization approach. One is a post-design analysis to understand the tradeoffs among the conflicting goals, while the second is the early-stage DSE before making final design decisions. In the first example, we discuss solution space exploration, where one has a set of samples and corresponding goal values obtained after running the cDSP, and, the designer needs to select samples based on the goals. iSOM provides plots of all goals of the design problem. This makes the selection of RoI convenient and the designer understands where in the solution space can the maximum number of goals be satisfied simultaneously and which all goals need to be compromised to meet

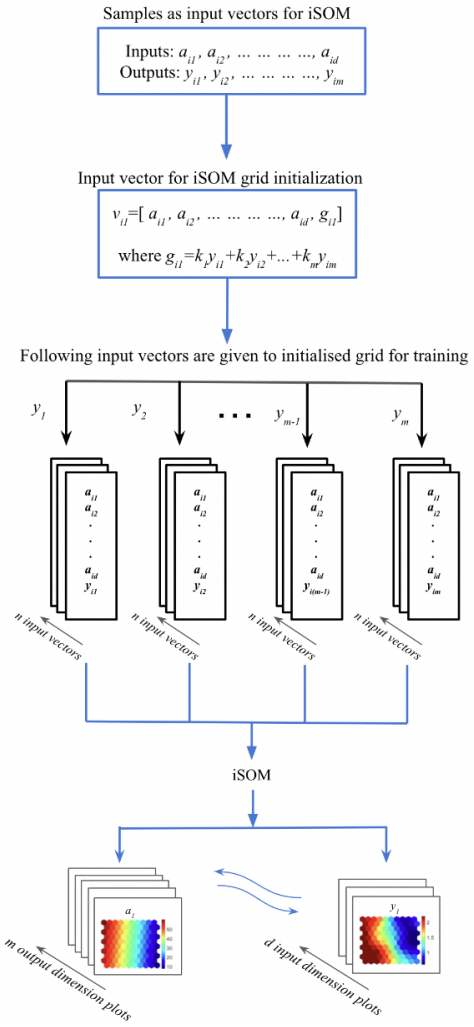

Fig. 3 Flow chart for the proposed design approach

the designer's requirement in the best possible manner. The second example discusses dealing with design space exploration during early stage design. Instead of sampling in the entire design space, which has a large computational cost associated with it, the present work shows how iSOM permits reducing the design space for further sampling during the later stages of design. This has been demonstrated using a car crash design problem which is known to be inherently complex in nature. The focus is to identify the regions in input space that corresponds to maximum risk by analyzing many neck and head injury metric plots generated using iSOM, thus leading to a more informed decision as the designer progresses further into the design.

4 TEST PROBLEM 1: THE HOT ROD ROLLING PROCESS CHAIN PROBLEM

Steel is one of the most widely used alloys globally and finds application across a large variety of sectors such as construction, automotive, shipbuilding, and refining [49]. In recent times, there has been a rising demand from customers for grades of steel that offer superior performance across different sectors, especially the automotive industry [49, 50]. This rising demand for newer steel grades with improved properties and performances poses a challenge for the steel manufacturing industry as they are required to design the steel manufacturing processing chain to yield the right microstructure and resultant properties that lead to better performance [51].

Hot Rod Rolling (HRR) is a manufacturing process used by steel industries to produce steel rods (semi-products) that are subsequently used to produce other artifacts or products, such as gear blanks. HRR system is characterized by a series of processes that are executed sequentially, starting at reheating steel obtained from the casting unit in the form of slabs or blooms followed by several passes of plastic deformation through rolling mills and cooling carried out in a run-out table, as represented in Figure 4. During the thermo-mechanical process, micro-structural evolution occurs in the material along with macro-structural changes, resulting in a steel rod with specific microstructural characteristics and corresponding mechanical properties.

In this paper, we consider a problem on the HRR of C-Mn steels for the production of steel rods, addressed by [10]. The original HRR problem formulation was composed of two separate sub-problems, the first for the structure-property relationships at the end of the cooling stage and the second for the process-structure relations during the rolling and cooling processing stages. In this paper, the original HRR problem formulation has been modified to account for the processing-structure-property relations in an integrated manner by combining the sub-problems into a single formulation where both the rolling and cooling processing stages are considered. For this use case, four important mechanical properties requirements that the semi-product needs to satisfy are identified and set as overall HRR system-level requirements. The requirements are to maximize the Yield Strength (YS), Tensile strength (TS), and Hardness (HV) of the rod and minimize the Impact Transition Temperature (ITT) of the material [10]. The steel microstructure design variables of the first sub-problem (Ferrite grain size after cooling - d_α, Pearlite interlamellar spacing after cooling - S_0, and Ferrite fraction after cooling - (X_f)) that determine the YS, TS, HV, and ITT mechanical properties of hot rolled steel rod material are set as functions of the design variables of the second sub-problem (steel composition, microstructure and processing variables: Carbon concentration [C], Manganese concentration after rolling [Mn], Austenite grain size after rolling [d_γ], and Cooling Rate [CR]). Hence, the mechanical properties are modeled as functions of the steel composition, steel microstructure, and processing design variables of the second sub-problem, thereby permitting the integrated consideration of processing-structure-property relations in the HRR test problem. The correlations between the material processing (during the cooling stage defined in terms of cooling rate (CR)), the microstructure of the steel (defined in terms of austenite grain size after rolling (d_γ); ferrite fraction (X_f), ferrite grain size (d_α), and pearlite interlamellar

spacing after cooling (S_0)), and the mechanical properties are studied in this problem. The cooling stage processing variable (cooling rate), the steel microstructure after the rolling process (austenite grain size), and elemental composition (in terms of C and Mn concentration) at the start of the cooling stage influence the steel microstructure achieved after the cooling process (identified in terms of ferrite grain size, ferrite fraction and pearlite interlamellar spacing). The steel microstructure after cooling defines the mechanical properties of the rod. Empirical models from the literature are used to define the processing-microstructure-property relations of the rod after the rolling and cooling process. One of the requirements identified is to manage the formation of banded microstructure, which includes alternate layers of ferrite and pearlite microstructures. The banded microstructure is one of the reasons for distortion in gear blanks. Therefore, a preferred Region of Interest (RoI) for the microstructure is one which has a high ferrite fraction (FF) or a high pearlite fraction region (corresponding to a low FF region). In the current work, constraints are defined for X_f, d_α, and S_0 to ensure that the microstructure generated after the rolling and cooling processes obeys the physical characteristics of the C-Mn steels and meets the microstructural requirements identified. The empirical models for these mechanical properties are listed in Table 1, and the empirical models for material microstructure achieved at the end of the cooling stage processing are listed in Table 2.

In the previous study by [52], ternary plots were used to visualize the solution space generated for the HRR design problem. Due to the limitations associated with visualization and exploring the solution space for more than three goals using ternary plots, only three of the mechanical property requirements (YS, TS, and HV) are considered as design goals in the multi-objective design problem formulated. The requirements on ITT and the steel microstructure are formulated as constraints in the previous study. Having the capability to consider these design requirements as goals and visualize their individual solution spaces will provide opportunities for the designer to explore and identify new and improved solution spaces that satisfice the many conflicting requirements of the problem. The capability will allow the designer to consider the interactions between the many goals and their relations with the many variables for the problem, allowing them to make informed design changes. From the problem perspective, the requirement is to study the solution space exploration of the multilevel manufacturing problem integrating the design of the material, product, and manufacturing processes, using an approach that: a) considers the multiple variables and the many-goal interactions, and b) helps identify solution regions of interest to generate satisficing design solutions for the many goals.

We view design as a decision-making process and use the compromise Decision Support Problem (cDSP) [53] construct to formulate the HRR problem. The design problem is formulated using the four keywords in the cDSP – Given, Find, Satisfy, and Minimize. We define targets for the four mechanical property goals in the cDSP. The designer seeks to achieve these targets using the cDSP by minimizing a deviation function that includes the deviations from the goal targets, defined as a weighted sum of individual goal deviations from their corresponding targets. The Adaptive Linear Programming (ALP) algorithm is used to solve the cDSP, executed in the DSIDES computational environment [54]. The details on solving the cDSP and the

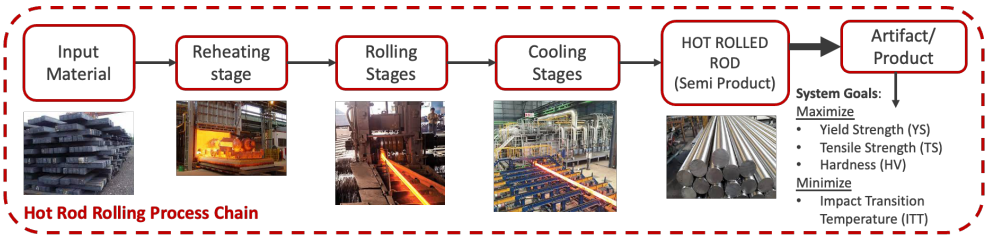

Fig. 4 The sequence of processes in steel manufacturing and the goals defined for the rod produced after rolling and cooling processes

ALP algorithm are available in [53] and are not repeated in this paper. The HRR problem cDSP reads as follows.

Given:

1. End requirements of HRR process in terms of Mechanical properties required
   (a) Goal G1: Maximize YS [MPa]
   (b) Goal G2: Maximize TS [MPa]
   (c) Goal G3: Maximize HV
   (d) Goal G4: Minimize ITT [K]
2. Well-established mathematical models for these properties in terms of the design variables (see Tables 1 and 2) and well-defined elemental composition (identified by P, Si, and N concentration - $[P]$, $[Si]$, and $[N]$).
3. Design Variables (X_j) and their bounds
   (a) X_1: Carbon concentration $[C]$ (%)
   (b) X_2: Manganese concentration after rolling $[Mn]$ (%)
   (c) X_3: Austenite grain size, d_γ (μm)
   (d) X_4: Cooling Rate, CR (K/s)

Find values of:

1. Design variables: X_j (for j = 1,...,4)
2. Deviation Variables: d_i (for d_1, d_2, d_3 and d_4)

Satisfy:

1. System Constraints
   (a) $220 \leq YS \leq 330$ (MPa)
   (b) $450 \leq TS \leq 750$ (MPa)
   (c) $131 \leq HV \leq 170$
   (d) $8 \leq d_\alpha \leq 25$ (μm)
   (e) $0.15 \leq S_0 \leq 0.25$ (μm)
   (f) $0.5 \leq X_f \leq 0.9$
   (g) $C_{eq} \leq 0.35$
   (h) $30 \leq d_\gamma \leq 100$ (μm)
   (i) $0.1833 \leq CR \leq 1.66$ (K/s)
2. System Goal:

(a) $YS(X_j)/YS_{target} + d_1^- - d_1^+ = 1$
(b) $TS(X_j)/TS_{target} + d_2^- - d_2^+ = 1$
(c) $HV(X_j)/HV_{target} + d_3^- - d_3^+ = 1$
(d) $ITT_{target}/ITT(X_j) + d_4^+ - d_4^- = 1$
where, $YS_{target} = 330$MPa, $TS_{target} = 750$MPa, $HV_{target} = 170$ And, $ITT_{target} = 293$K

3. Variable bounds
(a) $0.18 \leq X_1 \leq 0.3$ (%)
(b) $0.7 \leq X_2 \leq 1.5$ (%)
(c) $30 \leq X_3 \leq 100$ (μm)
(d) $0.1833 \leq X_4 \leq 1.66$ (K/s)

4. Deviation variable bounds
(a) $d_i^+, d_i^- \geq 0$
(b) $d_i^+ \times d_i^- = 0$

Minimize:
The deviation function Z is given as

$$\text{Min } Z = \sum W_i(d_i^+ + d_i^-) \tag{1}$$

where, $\sum W_i = 1$ and $i = 1, 2, 3, 4$

Table 1 Empirical models for mechanical properties in terms of microstructural characteristics at the end of the cooling process ([55–57]) (Average austenite to ferrite transition temperature, $T_{mf} = 700^oC$, Pearlite colony size, p = 6 μm, Carbide thickness, $t_{carb} = 0.025$ μm, $[N]$= 0.007%, $[Si] = 0.23\%$, $[P] = 0.024\%$)

Mechanical Property	Mathematical Model	Source
YS (MPa)	$X_f(77.7+59.9[Mn]+9.1(d_\alpha \times 0.001)^{-0.5})+478[N]^{0.5}+1200[P]+(1-X_f)(145.5+3.5S_0^{-0.5})$	Kuziac et.al.(1997) [55]
TS (MPa)	$X_f(20+2440[N]^{0.5}+18.5(0.001 \times d_\alpha)^{-0.5}+750(1-X_f)+3(1-X_f^{0.5})S_0^{-0.5}+92.5 \times [Si]$	Kuziac et.al.(1997) [55]
HV	$X_f(361-0.357T_{mf}+50[Si])+175(1-X_f)$	Yada(1987) [56]
ITT (K)	$273+X_f(-46-(11.5(d_\alpha \times 0.001)^{-0.5})+(1-X_f)(-335+(5.6 \times 0.001))S_0^{-0.5}-13.3p^{-0.5}+(3.48E6)\times(t_{carb}0.001)+49[Si]+762[N]^{0.5}$	Gladman et.al.(1972) [57]

The above cDSP formulation is exercised for different design scenarios to explore the design space and identify a set of satisficing design variable values (processing parameter, microstructure characteristics, and elemental concentrations) that meet the conflicting goals. These scenarios (45 scenarios, see Table 3 for sample scenarios) are created using the Latin Hypercube Sampling (LHS) design of experiments with

Table 2 Empirical models for microstructural characteristics at the end of the cooling stage processing ([58, 59])
(Assuming retained strain after the rolling process, $\epsilon_r = 0$)

End of cooling microstructure characteristics.	Mathematical Model	Source
Ferrite grain size, d_α	$(1-0.45\epsilon_r^{0.5})(-0.4+6.37C_{eq})+$ $(24.2–59C_{eq})CR^{-0.5}+22(1-e^{-0.015d_\gamma})$	Hodgson and Gibbs (1992) [59]
Pearlite interlamellar spacing, S_0	$0.1307 + 1.027[C] - 1.993[C]^2 - 0.1108[Mn] + 0.0305CR^{-0.52}$	Kuziac et.al.(1997) [58]
Ferrite fraction equivalent, $X_{f_{eq}}$	$1-([C]/(0.789-0.1671[Mn]+(0.1607[Mn]^2)-(0.0448[Mn]^3)))$	Kuziac et.al.(1997) [58]
Ferrite fraction, X_f	$X_{f_{eq}}-5.48(1-e^{(-0.0106CR)})-$ $(0.723(1-e^{(-0.0009d_\gamma)}))$	Kuziac et.al.(1997) [58]
Carbon equivalent, C_{eq}	$([C]+[Mn])/6$	Hodgson and Gibbs (1992) [59]

Table 3 Sample scenarios with weight for goals

Scenarios	**YS: W1**	**TS: W2**	**HV: W3**	**ITT: W4**
3	0.08	0.55	0.36	0.01
11	0.26	0.02	0.07	0.65
27	0.33	0.34	0.16	0.17
41	1	0	0	0
45	0.25	0.25	0.25	0.25

5 additional design points added based on the designer's judgment to effectively capture the solution space by assigning different weights to the four goals such that the sum of the weights equals one. The different weight values for the four goals represent the varying preferences of the designer amongst the four different goals, with a larger weight value indicating a higher priority or importance. The relevance and characteristics of some sample design scenarios are detailed in the next section, Section 4.1.

4.1 Integrated solution space exploration using iSOM for the HRR problem

Scenarios in Table 3 are selected so that the design space is sufficiently sampled for exploration using iSOM. We explain the significance of these scenarios using the cDSP for the end product. For the cDSP, scenario 3 represents a situation where the designer has different preferences for different goals. Scenario 11 represents a situation where one goal i.e., minimizing ITT, is given a very high preference over the others by the designer. A scenario where pairs of goals are given nearly equal preferences, with one pair of goals having a higher weightage over the other pair, is represented in scenario 27. Scenario 41 depicts a situation where the designer's interest is to achieve

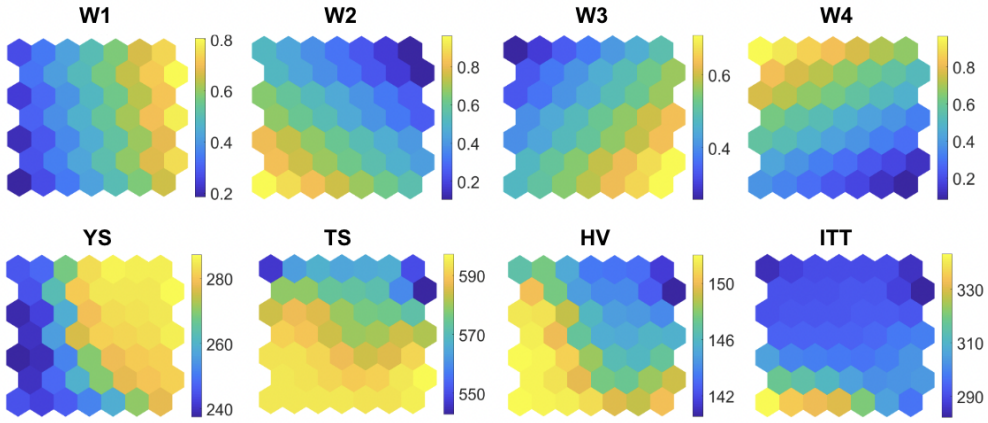

Fig. 5 Input and output component planes for the HRR problem

the target of a single goal i.e., maximizing YS, as closely as possible. Scenario 45 represents a situation where the designer gives equal preference to all the goals.

The weights shown in Table 3 are used in the deviation function of the cDSP formulation, as discussed above, as a weighted sum of individual goal deviations from their corresponding targets. Figure 5 shows the component planes of four output goals obtained with respect to weights given to each goal during the formulation of cDSP problem. As explained earlier, in the cDSP formulation, a deviation function that includes the deviations from the goal targets, defined as a weighted sum of individual goal deviations from their corresponding targets, is minimized. Here $W1$ corresponds to the weight given to YS, $W2$ to TS, $W3$ to HV, and $W4$ to ITT. Using the iSOM plots, designers will be able to understand the relations among input weights ($W1$ to $W4$) and corresponding cDSP goals. For example, it can be observed that when $W1$ or $W4$ is above 0.8, high values of YS and low values of ITT are obtained. Similarly, a high value of either $W2$ or $W3$ results in high values for both TS and HV. The iSOM plots also permit designers to understand the relations among the cDSP goals. For example, from the output component planes obtained using iSOM and presented in Figure 5 (see YS, TS, HV, and ITT iSOM plots), it is evident that high values of YS correspond to low values of TS and HV. Also, ITT and YS exhibit similar variation, and HV and TS also exhibit similar variation, but it is opposite to that of YS and ITT. Hence, one can observe the conflict in achieving all the goals, i.e., maximizing YS, TS, and HV and minimizing ITT simultaneously. In the section below, we discuss the approach to identifying feasible solutions as per the designer's requirement using iSOM visualization.

On analyzing the results in [10] for the mechanical property goals and requirements, it is observed that the Ferrite Fraction (FF) variable plays a key role in defining the mechanical properties. A major requirement is to manage the banded microstructure of ferrite and pearlite. This requirement can be satisfied by identifying regions with high FF or low FF (meaning high pearlite fraction). Hence, the component plane of FF, which is set as a constraint in the cDSP formulation, is plotted

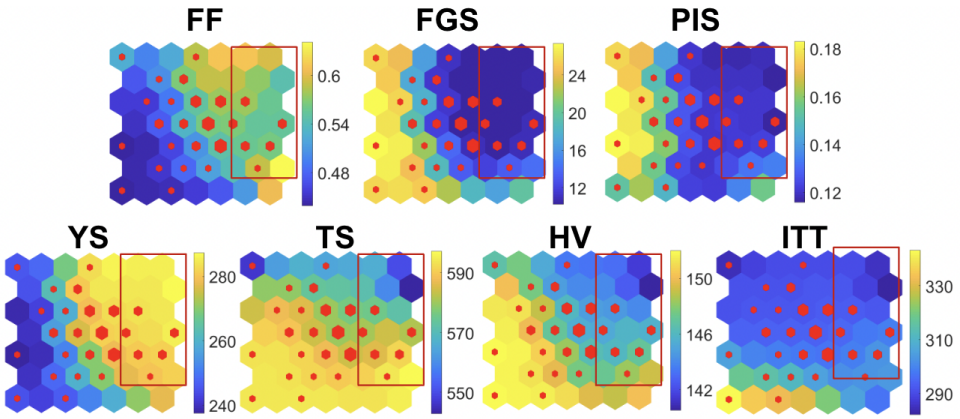

Fig. 6 RoI shown by the red rectangle and hits shown by red dots

in Figure 6. The Ferrite Grain Size (FGS) and Pearlite Interlamellar spacing (PIS) also influence the mechanical properties achieved, and hence constraints are placed in the cDSP formulation for these microstructural characteristics in order to achieve the required mechanical properties. The component planes for FGS and PIS are also plotted in Figure 6. Important design insights regarding the influence of material microstructural characteristics (other than the design variables) on the cDSP goals can be drawn from these iSOM plots. A high weightage on YS ($W1$) will result in high FF, low FGS, and low PIS. Similarly, a high weightage on TS ($W2$) will result in lower FF, and larger FGS and PIS. It is observed that the requirements for maximizing tensile strength and hardness are achieved in the high pearlite fraction region (i.e. low FF), while the requirements for maximizing yield strength and minimizing impact transition temperature are satisfied at the high ferrite fraction region. Hence, the designer is faced with the dilemma of choosing from either the region of high ferrite or high pearlite that satisfies the corresponding goals.

To make a decision, the region where FF is maximum is selected as RoI. The red rectangle in Figure 6 shows RoI on the ferrite component plane and the corresponding ranges in YS, TS, HV, and ITT component planes. The solution points are then identified by finding the sample points that fall in the RoI to analyze the extent to which the goals are met. The red dots indicate samples mapped to nodes. If a node gets selected as BMU, it is considered that the node has a hit. Depending on how many hits a node has the size of the red dot increases. A large number of hits implies more samples got mapped to that particular node. In the RoI, nodes that had hits correspond to 6 solution points. Results associated with each of these solution points are summarized in Table 4.

In [10], the ternary plots for individual goals and their superposed version were used to make design decisions. The ternary plot-based approach offers the limited capability to visualize the entire solution space, as only three goals can be studied at a time. Further, developing a superposed plot to explore the solution space is

Table 4 Solution points selected in RoI for HRR problem

SCENARIO	W1	W2	W3	W4	YS (MPa)	TS (MPa)	HV	ITT (K)	X_f (FF)	d_α (FGS) (μm)	S_0 (PIS) (μm)
1	0.46	0.23	0.23	0.08	282.34	582.51	145.59	297.45	0.56	9.93	0.12
28	0.32	0.09	0.49	0.1	275.78	604.35	148.88	316.04	0.49	9.91	0.11
32	0.35	0.19	0.34	0.12	280.61	589.58	146.59	302.05	0.54	9.84	0.12
37	0.37	0.05	0.33	0.25	284.26	573.34	144.35	282.81	0.58	10.11	0.12
41	1	0	0	0	289.58	527.82	139.01	276.6	0.68	11.95	0.11

tedious and cannot be easily interpreted. Most importantly, with the ternary plots, the designers are only able to visualize the relations between inputs and outputs of a single sub-problem, i.e., the sub-problem involving the microstructure-property relations. Ternary plots fail to assist designers in visualizing the relations between the processing, microstructure, and properties across the two sub-problems that involve the processing-microstructure and microstructure-property relations. iSOM-based solution space exploration addresses these limitations since one is able to visualize the solution space for problems characterized by many goals and requirements across multiple sub-problems and make design decisions by identifying RoI. The approach offers the capability to easily interpret regions of interest and determine the corresponding cDSP weight combinations that meet the designer's target or preference. In the case of the hot rod rolling problem, the requirements are to maximize the mechanical properties of the rod. However, based on the iSOM analysis, designers can observe that these goals are conflicting in nature, and a common region that satisfices all the goals simultaneously is not available. Using the iSOM-based solution space exploration carried out, the weight combinations that best satisfice the many-goal problems are identified.

The utility of the approach is that the designer can easily modify the design requirements and use the iSOM plots to select regions that meet a new design preference defined. For example, let's assume the design requirement for another designer is to achieve a high tensile strength for the steel product given the same problem requirements. In that situation, the designer can easily identify the high TS regions from the iSOM plots in Figure 6. These correspond to regions identified by the yellow color on the TS component plot. The same region corresponds to a high weight on Goal 2 ($W2$) and Goal 3 ($W3$) and a low weight on Goal 1 ($W1$) and Goal 4 ($W4$). The region also corresponds to a high pearlite fraction (identified as low FF values in the FF component plot). Thus, the designer is able to quickly make judgments regarding the weight combinations using the iSOM plots instead of carrying out a separate analysis. iSOM plots thus serve as a look-up table to be used by process designers to make informed decisions without actually running the simulations repeatedly, which in turn saves computational time and cost.

The iSOM-based visualization provides additional functionalities over ternary plots during design space exploration, as listed below, making it a suitable tool to support design space exploration.

Table 5 Critical intercept values used for normalization in calculation of lateral N_{ij} [63]

Variable	Intercept Value
F_{int} (Tension)	6810 N
F_{int} (Compression)	6160 N
M_{int} (Left)	60 Nm
M_{int} (Right)	60 Nm

Table 6 Crash variables and their bounds

Crash Variables	Lower Bound	Upper Bound
Impact Velocity (v) (mph)	10	45
Impact Location (ω) (degree)	0	360
Angle of Impact (θ) (degree)	0	360

1. Visualize the solution space for all the goals simultaneously without having to set any goal as a constraint (as in ternary plots when there are more than 3 goals)
2. Visualize the design space of important design variables, in addition to the goals.
3. Visualize the relations between the design spaces of related sub-problems.

When using the iSOM-based approach in the context of the HRR problem, the designer can formulate all four goals as goals themselves and is not required to formulate the ITT goal as a constraint. The designer is able to visualize the relations among the design spaces of sub-problems that involve the processing-microstructure and microstructure-property relations. With a better understanding of different correlations between the multiple goals/requirements and the variables for the problem (which are fully considered) across multiple related sub-problems, the designer is also more confident about the solutions obtained.

5 TEST PROBLEM 2: CAR CRASH PROBLEM

With 1.35 million deaths and up to 50 million injuries each year, vehicular accidents are a major contributor to the total number of global accident-related injuries [60]. It is, therefore, critical to understand injuries resulting from various crash scenarios. In this study, we utilize Finite Element (FE) models, surrogate models technique, and visualization using iSOM to investigate the effect of crash variables (impact velocity (v), impact location (ω), and angle of impact (θ)) on injury metrics. For studying injuries, Head Injury Criterion (HIC), Neck Injury Criteria (N_{ij}), and its derivatives (Lateral N_{ij} and N_{km}) are used. HIC is one of the most commonly used injury metrics for predicting head injury response which measures the likelihood of inducing injury as a factor of sustained linear acceleration [61, 62]. On the other hand, Neck Injury Criteria (N_{ij}) and its derivatives (Lateral N_{ij} and N_{km}) assess neck injury in terms of axial forces and moments at the occipital condyles.

5.1 Head Injury Metric Analysis

HIC is used as a criterion to assess the likelihood of inducing head injury [64]. The following equation is used to calculate HIC for all the crash scenarios [65]:

$$HIC = \max_{t_1,t_2} \left\{ (t_2 - t_1) \left[\frac{1}{t_2 - t_1} \int_{t_1}^{t_2} a(t)dt \right]^{2.5} \right\} \tag{2}$$

where a is the resultant linear acceleration (g) measured from the CG of the head of the THUMS model and $(t_2 - t_1)$ is a time duration (ms). HIC_{15} is calculated with a time duration of 15ms, and HIC_{36} is calculated with a time duration of 36ms. In this study, we use 15ms as time duration for all HIC calculations, as specified by NHTSA standards [63].

Table 7 Neck injury risk metrics and sub-metrics

Crash Scenarios	Front Impact	Rear Impact	Side Impact
	N_{ij}	N_{km}	$Lateral N_{ij}$
Metrics and	NTF	NFA	NTL
Submetrics	NTE	NEA	NTR
	NCF	NFP	NCL
	NCE	NEP	NCR

5.2 Neck Injury Metric Analysis

N_{ij} quantifies the neck injury risk within the neck of the driver for front impacts [62]. N_{ij} measures the likelihood of inducing four loading cases within the cervical spine with normalized axial forces and sagittal plane bending moments. The four sub-metrics representing these loading cases are tension-flexion (NTF), tension-extension (NTE), compression-flexion (NCF), and compression-extension (NCE) [66]. It utilizes the following equation in the calculation:

$$N_{ij} = \frac{F_Z}{F_{int}} + \frac{M_Y}{M_{int}} \tag{3}$$

where F_Z is the axial load (N) and M_Y is the sagittal bending moment (N_m) [63]. F_{int} and M_{int} are critical intercept values used to normalize the axial load and lateral plane bending moment (see Table 5).

As N_{ij} does not sufficiently capture injury risk in all crash scenarios, N_{km} and Lateral N_{ij} are calculated (for details; see [68]). N_{km} is developed to account for injury risk associated with low-speed rear impacts. N_{km} represents four sub-metrics that measure loading cases within the cervical spine: flexion-anterior shear (NFA), extension-anterior shear (NEA), flexion-posterior shear (NFP), and extension-posterior shear (NEP) [69]. To account for side impacts, Lateral N_{ij} is used. Lateral N_{ij} also represents four

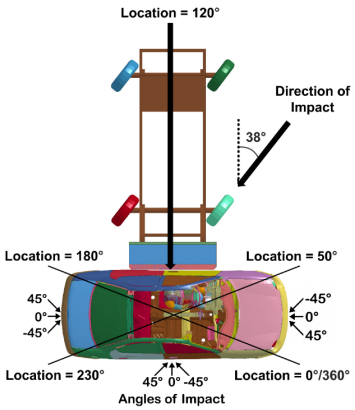

Fig. 7 Schematic showing the numerical orientations of the impact location and angle of impact variables with respect to the dodge neon FE model

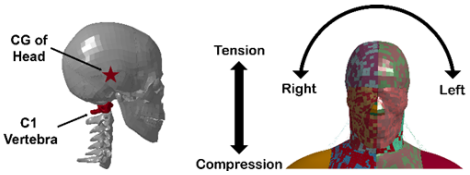

Fig. 8 Schematic showing the approach of obtaining the output data from the FE model [67]

loading cases that are measured using four sub-metrics, that are, tension-left lateral (NTL), tension-right lateral (NTR), compression-left lateral (NCL), and compression-right lateral (NCR) [70]. The summary of the metrics utilized to capture injury risk in different crash scenarios is tabulated in Table 7.

5.3 Finite Element Simulation Setup and Data Generation

The FE model consists of an occupant vehicle model, a human model, and an impacting vehicle model (see Figure 9). The locations (ω) are oriented radially from the center of the vehicle, starting from the front-far side corner (0°) and rotating counterclockwise for a full 360°. The front, near, rear, and far side are defined as between 0° and 50°, 50° and 180°, 180° and 230°, and 230° and 360°, respectively. The angle of impact (θ) spans from -45° to 45° and can be defined at any impact location. For visualization purposes, the angles of impact are shown at specific locations across the impact location range of 0° to 360°. A near-side car impact with the Moving Deformable Barrier (MDB) at an impact location of 120° and an angle of impact of 38° is also shown [67]. The occupant vehicle is a 1996 Dodge Neon created by the United States National Crash Analysis Center [71, 72] and modified by researchers at

the Center for Advanced Vehicular Systems (CAVS) at Mississippi State University [73, 74]. Within this vehicle, Version 4 adult male 50^{th} percentile Total Human Model for Safety (THUMS) is belted to the driver's seat using the three-point seat belt. Toyota Motor Corporation created this model to represent an adult human male of average height and weight [75, 76]. The impacting vehicle is an MDB model created by [74]. This model consists of a deformable aluminum honeycomb front bumper and a rigid chassis/frame [73, 77] and meets the safety standards specified by the National Highway Traffic Safety Administration (NHTSA) [78].

As shown in Figure 8, the resultant linear acceleration data required model for the calculation of the head injury metric is obtained from the Center of Gravity (CG) of the head of the THUMS. For the calculation of the neck injury metrics, forces and moments are obtained from the C1 vertebra of the THUMS model (see Figure 8). In-house Python scripts are used to obtain these data from the simulation output files.

5.4 Problem Formulation

Table 8 Second-order Surrogate Models for HIC_{15} and NIC

Injury Metrics	**Surrogate Models**
HIC$_{15}$	4330.8479 - 366.42336 * v + 58.405123 * θ + 24.0371 * ω + 6.1426506 * v^2 - 0.48959089 * θ^2 - 0.16011745 * ω^2 - 1.9191392 * v * θ + 0.38787089 * v * ω - 0.034891723 * θ * ω
NTL	-0.25276 - 0.023171 * v - 0.00052139 * θ + 0.01967 * ω + 0.00027869 * v^2 - 0.00030386 * θ^2 - 0.00010487 * ω^2 + 0.00010836 * v * θ + 0.0001704 * v * ω - 0.000020892 * θ * ω
NTR	-1.6258 + 0.067876 * v - 0.0056195 * θ + 0.015463 * ω - 0.00068404 * v^2 + 0.000026671 * θ^2 - 0.000052106 * ω^2 + 0.000006767 * v * θ - 0.00012076 * v * ω + 0.000020693 * θ * ω
NCL	-0.60187 - 0.051335 * v + 0.0047267 * θ + 0.035072 * ω + 0.00059986 * v^2 - 0.00039911 * θ^2 - 0.00018029 * ω^2 + 0.00013257 * v * θ + 0.00029284 * v * ω - 0.000063187 * θ * ω
NCR	-1.975 + 0.039712 * v - 0.00037145 * θ + 0.030865 * ω - 0.00036288 * v^2 - 0.000068583 * θ^2 - 0.00012753 * ω^2 + 0.000030982 * v * θ + 0.0000016813 * v * ω - 0.00002160 * θ * ω

We are investigating injury concerns resulting from car crashes, specifically focusing on HIC and Lateral N_{ij} as design goals to assess injuries (refer to Table 7) during a car crash. By manipulating crash variables such as impact angle, impact location, and impact velocity, we generate various crash scenarios. Visualizing the solutions becomes challenging due to the combination of five design goals and two crash vehicles. To effectively explore different crash conditions and identify potential injury concerns, iSOM visualization technique has been used. It acts as a valuable decision support tool which allows us to study the interaction between design goals and their relationship with the crash variables.

The study utilizes crash variables, which are listed in Table 6, to conduct a total of 97 crash scenarios using a Latin hypercube design. Each scenario is simulated using LS-DYNA software (LSTC, Livermore, CA, USA). Figure 8 illustrates an example crash scenario where the FE MDB model collides with the Dodge Neon vehicle model at an impact location of 120° and an impact angle of 38°. The results obtained from

these crash scenarios are then used to develop second-order polynomial surrogate models that establish the relationship between the crash conditions and injury matrices, see Table 8. We use the multivariate polynomial regression method to develop the surrogate models and employ the coefficient of determination (R-squared) and Cross-Validated Mean Absolute Error (CVMAE) as the goodness of fit measures, see Table 9. With the aid of these surrogate models, a many-goal constrained cDSP is formulated. The formulation of the multigoal cDSP for the problem is presented below. The cDSP formulation is characterized by the presence of 5 goals and 2 design variables, with the impact location variable assumed to be fixed at 120 degrees for a side impact scenario.

Table 9 Error Metrics of Surrogate Models for HIC_{15} and NIC

Injury Metrics	**R-squared**	**CVMAE**
HIC$_{15}$	0.8703	3.0502
NTL	0.8505	0.4055
NTR	0.7911	0.2376
NCL	0.8985	0.4781
NCR	0.9312	0.2741

Given:

1. Information specific to the car crash problem. Assumption: Impact Location, $\omega = 120$
2. Design variables (X_p) and their bound:
   (a) $25 \leq X_1$: Impact Velocity, v (mph) ≤ 45
   (b) -45 $\leq X_2$: Impact Angle, θ (degrees) ≤ 45
3. Goals (G_i) and goal targets:
   (a) Goal G_1: Maximize HIC_{15}
   (b) Goal G_2: Maximize NTL
   (c) Goal G_3: Maximize NCR
   (d) Goal G_4: Maximize NTR
   (e) Goal G_5: Maximize NCL
4. Models that relate the design variable and goals, see surrogate models in Table 8 .

Find values of

1. Design variables: X$_p$ (for j = 1,2)
2. Deviation Variables: d_i (for d_1, d_2, d_3, d_4 and d_5)

Satisfy

1. System Constraints
   (a) $0 \leq HIC_{15} \leq 5200$
   (b) $0 \leq$ NTL ≤ 1.4
   (c) $0 \leq$ NCR ≤ 1.2
   (d) $0 \leq$ NTR ≤ 1
   (e) $0 \leq$ NCL ≤ 1.9

2. System Goal:
   (a) $G_1/G_{1_{target}} + d_1^- - d_1^+ = 1$
   (b) $G_2/G_{2_{target}} + d_2^- - d_2^+ = 1$
   (c) $G_3/G_{3_{target}} + d_3^- - d_3^+ = 1$
   (d) $G_4/G_{4_{target}} + d_4^+ - d_4^- = 1$
   (e) $G_5/G_{5_{target}} + d_5^+ - d_5^- = 1$
   where, Goal Targets:
   $G_{1_{target}} = 800$; $G_{2_{target}} = 0.8$; $G_{3_{target}} = 0.8$; $G_{4_{target}} = 0.8$; $G_{5_{target}} = 0.8$
3. Variable bounds
   (a) $25 \leq$ X_1 (mph) ≤ 45
   (b) -45 $\leq$ X_2 (degrees) $\leq$ -45
4. Deviation variable bounds
   (a) $d_i^+, d_i^- \geq 0$
   (b) $d_i^+ \times d_i^- = 0$

Minimize
The deviation function Z given as

$$Min\ Z = \sum W_i(d_i^+ + d_i^-) \tag{4}$$

where, $\sum W_i = 1$ and $i = 1, 2, 3, 4, 5$

The multigoal cDSP formulation presented above is exercised for different design scenarios to generate the different design solutions for the problem. A total of 36 design scenarios are created by changing the assigned weights to the design goals. The 36 design solutions corresponding to the 36 design scenarios are then used to generate plots using the proposed design methodology, allowing for an analysis of how different combinations of input variables impact the head and neck injury metrics. In the next section we focus on discussing the insights and conclusions drawn from the importance inferences derived from the iSOM visualization.

5.5 Solution space exploration for car crash problem using iSOM

The plots generated are displayed in Figure 9 and Figure 10. Figure 9 presents the output component places representing the head and neck injury metrics in relation to the input component planes, which correspond to the weights assigned to the goals

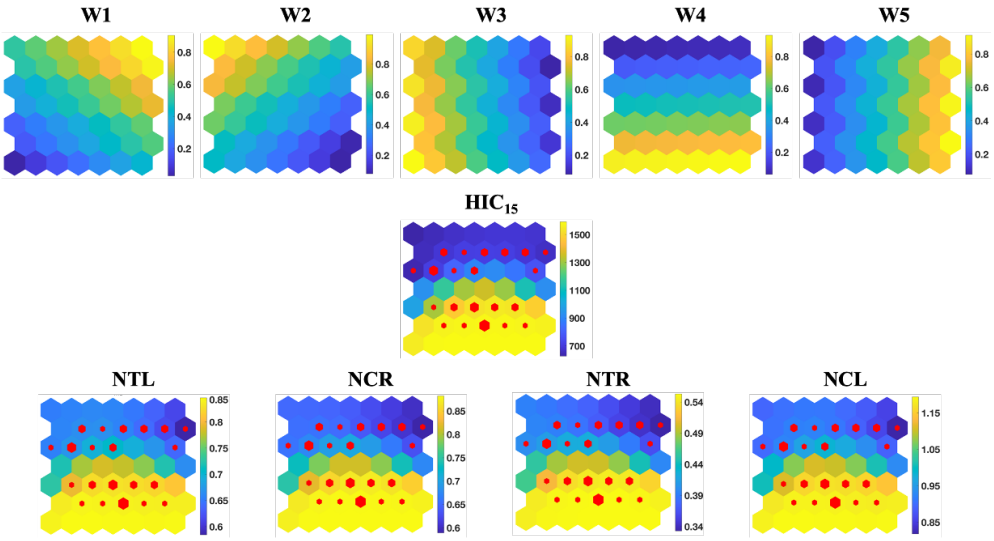

Fig. 9 Inputs and output component planes for car crash problem

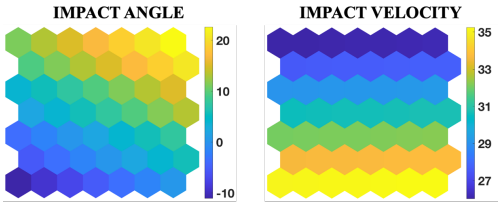

Fig. 10 Component planes of design variables for car crash problem

in the cDSP formulation. The weights are denoted as W_1 for HIC_{15}, W_2 for NTL, W_3 for NCR, W_4 for NTR, and W_5 for NCL. The plots reveal that the injury metrics exhibit similar trends to the component plane of W_4, indicating that a higher value of this weight results in elevated injury metric values. This suggests a stronger influence of NTR on the other injury metrics. Hence, the iSOM plots aid the identification of critical goals and their influence on the other goals of a design problem.

Furthermore, identifying high-risk regions is of interest. To illustrate how this identification can be discussed using the plots, the RoI is defined as having high head injury metric values (greater than 1000), as shown in Figure. 11. The red box highlights the RoI, indicating that higher head injury values correspond to elevated neck injury values. By examining the design variables plots of impact angle and impact velocity within the marked RoI (as seen in Figure 11), the critical ranges of these variables that contribute to maximum injury can be identified. In this case, the critical range for impact angle lies between -10 and +5 degrees, while for impact velocity, it is between 32 and 35 mph. Hence, the iSOM plots can be used by decision-makers to assess the impacts of variables on the goals of the car crash problem and vice-versa.

The red dots on the nodes of the component plane in Figure 11 represent samples that are mapped to those nodes. The red rectangle representing the RoI contains some

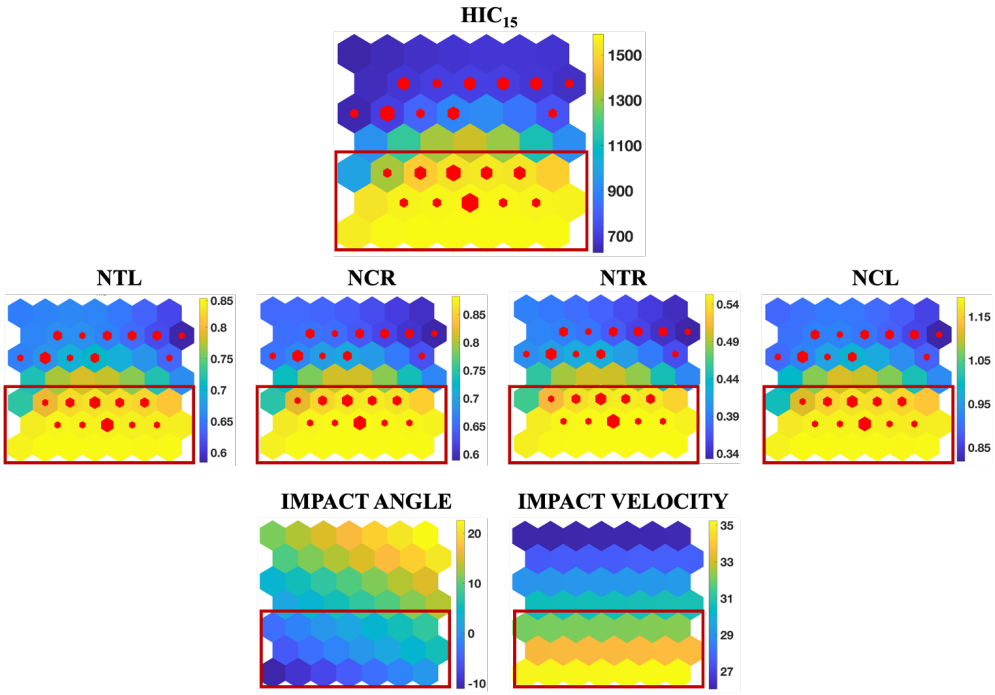

Fig. 11 RoI shown by red rectangles and hits shown by red dots

Table 10 Solution points selected in RoI for car crash problem

SCENARIO	W1	W2	W3	W4	W5	v	θ	ω	HIC_{15}	NTL	NCR	NTR	NCL
4	0	0	0	1	0	36.9234	-7.90175	120	1574.04	0.85	0.88	0.54	1.19
6	0.2	0.2	0.2	0.2	0.2	36.5723	-10.1039	120	1538.27	0.83	0.88	0.55	1.16
7	0.25	0.25	0.25	0.25	0	36.5723	-10.1039	120	1538.27	0.83	0.88	0.55	1.16
8	0	0.25	0.25	0.25	0.25	36.9234	-7.90175	120	1574.04	0.85	0.88	0.54	1.19
9	0.25	0	0.25	0.25	0.25	36.5723	-10.3531	120	1539.76	0.83	0.88	0.55	1.16
10	0.25	0.25	0	0.25	0.25	36.5723	-10.1039	120	1538.27	0.83	0.88	0.55	1.16
13	0	0.33	0.34	0.33	0	36.9234	-7.90175	120	1574.04	0.85	0.88	0.54	1.19
14	0	0	0.33	0.34	0.33	36.9234	-7.90175	120	1574.04	0.85	0.88	0.54	1.19
15	0.33	0	0	0.33	0.34	36.5723	-10.3531	120	1539.76	0.83	0.88	0.55	1.16
19	0	0	0.5	0.5	0	36.9234	-7.90175	120	1574.04	0.85	0.88	0.54	1.19
20	0	0	0	0.5	0.5	36.9234	-7.90175	120	1574.04	0.85	0.88	0.54	1.19
24	0	0	0.25	0.75	0	36.9234	-7.90175	120	1574.04	0.85	0.88	0.54	1.19
25	0	0	0	0.25	0.75	36.9234	-7.90175	120	1574.04	0.85	0.88	0.54	1.19
29	0	0	0.75	0.25	0	36.9234	-7.90175	120	1574.04	0.85	0.88	0.54	1.19
30	0	0	0	0.75	0.25	36.9234	-7.90175	120	1574.04	0.85	0.88	0.54	1.19
33	0	0.2	0.4	0.4	0	36.9234	-7.90175	120	1574.04	0.85	0.88	0.54	1.19
34	0	0	0.2	0.4	0.4	36.9234	-7.90175	120	1574.04	0.85	0.88	0.54	1.19
35	0.4	0	0	0.2	0.4	36.5723	-10.3531	120	1539.76	0.83	0.88	0.55	1.16

red dots, which correspond to the scenarios falling within our RoI. These scenarios can be further sampled to investigate the significance of different neck injury metrics on head injury metrics. Table 10 provides information on the scenarios falling within the RoI.

The utilization of iSOM for solution space exploration demonstrates an enhanced visualization technique for analysis. Previous studies, such as [79] and [80], have separately investigated the effects of changing design variable values on neck and head injury metrics. However, these injury metrics have not been studied and analyzed together with the design variables. Additionally, previous works used contour plots to observe the influence of design variables on injury metrics, resulting in multiple contour plots that needed to be studied simultaneously to draw conclusions. In contrast, using iSOM accelerates and improves the information assessment process, enabling better decision-making with a broader range of available information. It also opens up avenues for further exploration of iSOM's utility for similar problems, providing opportunities for introspection and advancements in this field.

6 CLOSING REMARKS

In this paper, we propose an approach that combines iSOM visualization with the cDSP construct to support designers in carrying out design/solution space exploration for design problems with many conflicting goals and identify ranged set of satisficing solutions. The iSOM-based visualization allows for better understanding of the trade-offs among conflicting goals and the relations between design variables and goals, thereby supporting informed decision-making. The efficacy of the proposed iSOM-based approach in supporting design/solution space exploration to identify a ranged set of satisficing solutions is demonstrated using the hot rod rolling (HRR) process chain design problem and the car crash problem. Using the HRR process chain design problem, we demonstrate the ability of the proposed approach in supporting designers to better understand the influence of variables other than design variables on the conflicting goals, the trade offs between many (four) conflicting goals, and explore the design/solutions spaces to identify a ranged set of satisficing solutions. The car crash problem is used to demonstrate the ability of the proposed approach in supporting decision-makers to better understand the relations between variables (two) and many goals (five) and identify critical goals and assess their influence on other goals to help make informed decisions. Using these test examples, we demonstrate the capabilities offered by the proposed approach, which include the ability to: i) visualize and interpret many-goal problems and associated solution spaces in a cDSP framework, ii) establish relations between the input variables and output responses, and identify regions of interest, iii) explore regions of interest and identify satisficing solution regions that meet conflicting requirements, and iv) make informed decisions from the solution regions identified.

The proposed approach can be expanded to support robust design of systems with many conflicting goals, where the focus is on identifying ranged set of robust satisficing solutions that are relatively insensitive to uncertainties while still meeting the designers requirements. The robust design can be realized by combining iSOM visualization with the cDSP and robust design constructs like Design Capability Index (DCI) [81] and Error Margin Index (EMI) [82]. The proposed approach can also be used to support the visualization and simultaneous exploration of design spaces across multiple levels of decision-making, thereby supporting the concurrent design of multilevel systems. This

can be achieved by combining iSOM visualization with the coupled cDSP construct [83] and the Preemptive formulation [53].

7 Competing interests

The authors have no competing interests as defined by Springer, or other interests that might be perceived to influence the results and/or discussion reported in this paper

8 Acknowledgments and funding information

Rashmi Rama Sushil and Palaniappan Ramu thank IIT Madras for the support. Mathew Baby and Anand Balu Nellippallil gratefully acknowledge the support from the National Science Foundation (Grant No. 2301808) and the Department of Mechanical and Civil Engineering, Florida Institute of Technology (FIT). Gehendra Sharma would like to acknowledge the support of Center for Advanced Vehicular Systems (CAVS). However there are no direct funding received for this work.

9 Replication of results

The 2 examples presented take data from [10] and [70,71]. The codes for generating the iSOM plots are available upon request.

References

[1] Chu, X.-Z., Gao, L., Qiu, H.-B., Li, W.-D., Shao, X.-Y.: An expert system using rough sets theory and self-organizing maps to design space exploration of complex products. Expert Systems with Applications **37**(11), 7364–7372 (2010)

[2] Ayesha, S., Hanif, M.K., Talib, R.: Overview and comparative study of dimensionality reduction techniques for high dimensional data. Information Fusion **59**, 44–58 (2020)

[3] Keim, D.A.: Visual exploration of large data sets. Communications of the ACM **44**(8), 38–44 (2001)

[4] Richardson, T., Kannan, H., Bloebaum, C.L., Winer, E.H.: Incorporating value-driven design into the visualization of design spaces using contextual self-organizing maps: A case study of satellite design. In: 15th AIAA/ISSMO Multidisciplinary Analysis and Optimization Conference, p. 2728 (2014)

[5] Shavazipour, B., López-Ibáñez, M., Miettinen, K.: Visualizations for decision support in scenario-based multiobjective optimization. Information Sciences **578**, 1–21 (2021)

[6] Nagar, D., Ramu, P., Deb, K.: Visualization and analysis of pareto-optimal fronts using interpretable self-organizing map (isom). Swarm and Evolutionary Computation **76**, 101202 (2023)

[7] Simpson, T.W., Miller, S., Tibor, E.B., Yukish, M.A., Stump, G., Kannan, H., Mesmer, B., Winer, E.H., Bloebaum, C.L.: Adding value to trade space exploration when designing complex engineered systems. Systems Engineering **20**(2), 131–146 (2017)

[8] Sabeghi, M., Smith, W., Allen, J.K., Mistree, F.: Solution space exploration in model-based realization of engineered systems. In: International Design Engineering Technical Conferences and Computers and Information in Engineering Conference, vol. 57076, pp. 02–03015 (2015). American Society of Mechanical Engineers

[9] Balu Nellippallil, A., Berthelson, P.R., Peterson, L., Prabhu, R.K.: Head and neck injury risk criteria-based robust design for vehicular crashworthiness. In: International Design Engineering Technical Conferences and Computers and Information in Engineering Conference, vol. 84010, pp. 11–11015 (2020). American Society of Mechanical Engineers

[10] Nellippallil, A.B., Rangaraj, V., Gautham, B., Singh, A.K., Allen, J.K., Mistree, F.: An inverse, decision-based design method for integrated design exploration of materials, products, and manufacturing processes. Journal of Mechanical Design **140**(11) (2018)

[11] Miller, S.W., Simpson, T.W., Yukish, M.A., Stump, G., Mesmer, B.L., Tibor, E.B., Bloebaum, C.L., Winer, E.H.: Toward a value-driven design approach for complex engineered systems using trade space exploration tools. In: International Design Engineering Technical Conferences and Computers and Information in Engineering Conference, vol. 46315, pp. 02–03052 (2014). American Society of Mechanical Engineers

[12] Wang, Y., Huang, H., Rudin, C., Shaposhnik, Y.: Understanding how dimension reduction tools work: an empirical approach to deciphering t-sne, umap, trimap, and pacmap for data visualization. arXiv preprint arXiv:2012.04456 (2020)

[13] Johansson, J., Forsell, C.: Evaluation of parallel coordinates: Overview, categorization and guidelines for future research. IEEE transactions on visualization and computer graphics **22**(1), 579–588 (2015)

[14] Sobester, A., Forrester, A., Keane, A.: Engineering Design Via Surrogate Modelling: a Practical Guide. John Wiley & Sons, ??? (2008)

[15] Liu, S., Maljovec, D., Wang, B., Bremer, P.-T., Pascucci, V.: Visualizing high-dimensional data: Advances in the past decade. IEEE Transactions on Visualization and Computer Graphics **23**(3), 1249–1268 (2017) https://doi.org/10.1109/TVCG.2016.2640960

[16] Oakley, D.R., Sues, R.H., Rhodes, G.S.: Performance optimization of multidisciplinary mechanical systems subject to uncertainties. Probabilistic Engineering

Mechanics **13**(1), 15–26 (1998)

[17] Sues, R.H., Oakley, D.R., Rhodes, G.S.: Multidisciplinary stochastic optimization. In: Engineering Mechanics, pp. 934–937 (1995). ASCE

[18] Du, X., Chen, W.: Efficient uncertainty analysis methods for multidisciplinary robust design. AIAA Journal **40**, 545–552 (2002) https://doi.org/10.2514/3.15095

[19] Gu, X., Renaud, J.E., Batill, S.M., Brach, R.M., Budhiraja, A.: Worst case propagated uncertainty of multidisciplinary systems in robust design optimization. Structural and Multidisciplinary Optimization **20**, 190–213 (2000) https://doi.org/10.1007/s001580050148

[20] Kim, H.M., Michelena, N.F., Papalambros, P.Y., Jiang, T.: Target cascading in optimal system design. J. Mech. Des. **125**(3), 474–480 (2003)

[21] Kroo, I., Altus, S., Braun, R., Gage, P., Sobieski, I.: Multidisciplinary optimization methods for aircraft preliminary design. In: 5th Symposium on Multidisciplinary Analysis and Optimization, p. 4325 (1994)

[22] Sobieszczanski-Sobieski, J., Kodiyalam, S.: Bliss/s: a new method for two-level structural optimization. Structural and Multidisciplinary Optimization **21**, 1–13 (2001)

[23] Shahan, D.W., Seepersad, C.C.: Bayesian network classifiers for set-based collaborative design (2012)

[24] Simon, H.: Administrative behavior, McMillan, New York. Thompson, JD (1967), Organizations in actions. McGraw-Hill, New York (1947)

[25] Simon, H.A.: Rational choice and the structure of the environment. Psychological review **63**(2), 129 (1956)

[26] Mistree, F., Smith, W., Bras, B., Allen, J., Muster, D., *et al.*: Decision-based design: a contemporary paradigm for ship design. Transactions, Society of Naval Architects and Marine Engineers **98**(1990), 565–597 (1990)

[27] Muster, D., Mistree, F.: The decision support problem technique in engineering design. The International Journal of Applied Engineering Education **4**, 23–33 (1988)

[28] Mistree, F., Bras, B., Hughes, O.F.: Compromise decision support problem and the adaptive linear programming algorithm. Structural Optimization: Status Promise, 247–286 (1993)

[29] Choi, H., McDowell, D.L., Allen, J.K., Rosen, D., Mistree, F.: An inductive design exploration method for robust multiscale materials design. Journal of Mechanical

Design, **130**, 031402 (2008)

[30] Nellippallil, A.B., Mohan, P., Allen, J.K., Mistree, F.: An inverse, decision-based design method for robust concept exploration. Journal of Mechanical Design **142**(8), 081703 (2020)

[31] Qin, X., Luo, Y., Tang, N., Li, G.: Making data visualization more efficient and effective: a survey. The VLDB Journal **29**, 93–117 (2020)

[32] Obayashi, S., Sasaki, D.: Visualization and data mining of pareto solutions using self-organizing map. In: International Conference on Evolutionary Multi-Criterion Optimization, pp. 796–809 (2003). Springer

[33] Parashar, S., Pediroda, V., Poloni, C.: Self organizing maps (som) for design selection in robust multi-objective design of aerofoil. In: 46th AIAA Aerospace Sciences Meeting and Exhibit, p. 914 (2008)

[34] Ito, K., Couckuyt, I., d'Ippolito, R., Dhaene, T.: Design space exploration using self-organizing map based adaptive sampling. Applied Soft Computing **43**, 337–346 (2016)

[35] Qiu, H., Xu, Y., Gao, L., Li, X., Chi, L.: Multi-stage design space reduction and metamodeling optimization method based on self-organizing maps and fuzzy clustering. Expert Systems with Applications **46**, 180–195 (2016)

[36] Thole, S.P., Ramu, P.: Design space exploration and optimization using self-organizing maps. Structural and Multidisciplinary Optimization **62**(3), 1071–1088 (2020)

[37] Baby, M., Guptan, A., Broussard, J., Allen, J.K., Mistree, F., Nellippallil, A.B.: A decision support framework for robust multilevel co-design exploration of manufacturing supply networks. Journal of Mechanical Design **146**(11) (2024)

[38] Baby, M., Rama Sushil, R., Ramu, P., Allen, J.K., Mistree, F., Nellippallil, A.B.: Robust, co-design exploration of multilevel product, material, and manufacturing process systems. Integrating Materials and Manufacturing Innovation **13**(1), 14–35 (2024)

[39] Yin, H.: The self-organizing maps: background, theories, extensions and applications. In: Computational Intelligence: A Compendium, pp. 715–762. Springer, ??? (2008)

[40] Kohonen, T., Somervuo, P.: Self-organizing maps of symbol strings. Neurocomputing **21**(1-3), 19–30 (1998)

[41] Vesanto, J.: Som-based data visualization methods. Intelligent data analysis **3**(2), 111–126 (1999)

[42] Vesanto, J.: Som-based data visualization methods. Intelligent data analysis **3**(2), 111–126 (1999)

[43] Witowski, K., Liebscher, M., Goel, T.: Decision making in multi-objective optimization for industrial applications–data mining and visualization of pareto data. In: Proceedings of the 7th European LS-DYNA Conference, Salzburg, Austria (2009)

[44] Qiu, H., Xu, Y., Gao, L., Li, X., Chi, L.: Multi-stage design space reduction and metamodeling optimization method based on self-organizing maps and fuzzy clustering. Expert Systems with Applications **46**, 180–195 (2016)

[45] Ito, K., Dhaene, T., El Masri, N., d'Ippolito, R., Peer, J.: Self-organizing map based adaptive sampling. In: 5th International Conference on Experiments/Process/System Modeling/Simulation/Optimization (IC-EpsMsO-2013), vol. 2, pp. 504–513 (2013)

[46] Suzuki, N., Okamoto, T., Koakutsu, S.: Visualization of pareto optimal solution sets using the growing hierarchical self-organizing maps. Electronics and Communications in Japan **100**(1), 3–17 (2017)

[47] Nagar, D., Ramu, P., Deb, K.: Interpretable self-organizing maps (isom) for visualization of pareto front in multiple objective optimization. In: International Conference on Evolutionary Multi-Criterion Optimization, pp. 645–655 (2021). Springer

[48] Vesanto, J., Himberg, J., Alhoniemi, E., Parhankangas, J.: Self-organizing map in matlab: the som toolbox. (1999). https://api.semanticscholar.org/CorpusID:15746005

[49] Baluch, N., Udin, Z.M., Abdullah, C.S.: Advanced high strength steel in auto industry: an overview. Engineering, Technology & Applied Science Research **4**(4), 686–689 (2014)

[50] Jin, Y.: Development of advanced high strength steels for automotive applications. La Metallurgia Italiana (2011)

[51] Olson, G.B.: Computational design of hierarchically structured materials. Science **277**(5330), 1237–1242 (1997)

[52] Nellippallil, A.B., Rangaraj, V., Gautham, B., Singh, A.K., Allen, J.K., Mistree, F.: A goal-oriented, inverse decision-based design method to achieve the vertical and horizontal integration of models in a hot rod rolling process chain. In: International Design Engineering Technical Conferences and Computers and Information in Engineering Conference, vol. 58134, pp. 02–03003 (2017). American Society of Mechanical Engineers

[53] Hughes, O.F.: Compromise decision support problem and the adaptive linear programming algorithm. Progress In Astronautics and Aeronautics: Structural Optimization: Status and Promise **150**, 251 (1993)

[54] Reddy, R., Smith, W., Mistree, F., Bras, B., Chen, W., Malhotra, A., Badhrinath, K., Lautenschlager, U., Pakala, R., Vadde, S.: Dsides User Manual. Systems Realization Laboratory. Woodruff School of Mechanical Engineering, Georgia Institue of Technology ... (1996)

[55] Kuziak, R., Cheng, Y., Glowacki, M., Pietrzyk, M.: Modeling of the microstructure and mechanical properties of steels during thermomechanical processing. technical note. Technical report, National Inst. of Standards and Technology (MSEL), Boulder, CO (United ... (1997)

[56] Yada, H.: Prediction of microstructural changes and mechanical properties in hot strip rolling. In: Proceedings of the Metallurgical Society of the Canadian Institute of Mining and Metallurgy, pp. 105–119. Elsevier, ??? (1988)

[57] Gladman, T., FB, P.: Some aspects of the structure-property relationships in high-carbon ferrite-pearlite steels (1972)

[58] Kuziak, R., Cheng, Y.-W., Glowacki, M., Pietrzyk, M.: Modeling of the microstructure and mechanical properties of steels during thermomechanical processing. NIST Technical Note(USA) **1393**, 72 (1997)

[59] PD, H.: A mathematical model to predict the mechanical properties of hot rolled c-mn and microalloyed steels. ISIJ international **32**(12), 1329–1338 (1992)

[60] Organization, W.H.: Global Status Report on Road Safety 2015. World Health Organization, ??? (2015)

[61] Henn, H.-W.: Crash tests and the head injury criterion. Teaching mathematics and its applications **17**(4), 162–170 (1998)

[62] Kleinberger, M., Sun, E., Eppinger, R., Kuppa, S., Saul, R.: Development of improved injury criteria for the assessment of advanced automotive restraint systems. NHTSA Docket **4405**(9), 12–17 (1998)

[63] Soltis, S.: An overview of existing and needed neck impact injury criteria for sideward facing aircraft seats. In: The Third Triennial International Aircraft Fire and Cabin Safety Research Conference, vol. 12 (2001)

[64] Berthelson, P., Ghassemi, P., Wood, J., Stubblefield, G., Al-Graitti, A., Jones, M., Horstemeyer, M.F., Chowdhury, S., Prabhu, R.: A finite element–guided mathematical surrogate modeling approach for assessing occupant injury trends across variations in simplified vehicular impact conditions. Medical & Biological Engineering & Computing **59**(5), 1065–1079 (2021)

[65] Versace, J.: A review of the severity index (1971)

[66] Eppinger, R., Kuppa, S., Saul, R., Sun, E.: Supplement: development of improved injury criteria for the assessment of advanced automotive restraint systems: Ii (2000)

[67] Nellippallil, A.B., Berthelson, P.R., Peterson, L., Prabhu, R.: A computational framework for human-centric vehicular crashworthiness design and decision-making under uncertainty. ASCE-ASME J Risk and Uncert in Engrg Sys Part B Mech Engrg (2022)

[68] Berthelson, P.R., Ghassemi, P., Wood, J.W., Liu, Y., Al-Graitti, A.J., Jones, M.D., Chowdhury, S., Prabhu, R.K.: Evaluation of occupant neck injury response to varied impact conditions using a finite element-mathematical surrogate modeling approach. International Journal of Crashworthiness, 1–17 (2021)

[69] Muser, M., Walz, F., Niederer, P., et al.: Nkm-a proposal for a neck protection criterion for low-speed rear-end impacts. Traffic Injury Prevention **3**(2) (2002)

[70] Soltis, S.J.: The third triennial international aircraft fire and cabin safety research conference october 22–25, 2001 an overview of existing and needed neck impact injury criteria for sideward facing aircraft seats (2001)

[71] Zaouk, A., Marzougui, D., Bedewi, N.: Development of a detailed vehicle finite element model part i: Methodology. International Journal of Crashworthiness **5**(1), 25–36 (2000)

[72] Zaouk, A., Marzougui, D., Kan, C.-D.: Development of a detailed vehicle finite element model part ii: Material characterization and component testing. International Journal of Crashworthiness **5**(1), 37–50 (2000)

[73] Horstemeyer, M., Ren, X., Fang, H., Acar, E., Wang, P.: A comparative study of design optimisation methodologies for side-impact crashworthiness, using injury-based versus energy-based criterion. International Journal of Crashworthiness **14**(2), 125–138 (2009)

[74] Fang, H., Rais-Rohani, M., Liu, Z., Horstemeyer, M.: A comparative study of metamodeling methods for multiobjective crashworthiness optimization. Computers & structures **83**(25-26), 2121–2136 (2005)

[75] Iwamoto, M., Kisanuki, Y., Watanabe, I., Furusu, K., Miki, K., Hasegawa, J.: Development of a finite element model of the total human model for safety (thums) and application to injury reconstruction. In: Proceedings of the International IRCOBI Conference, pp. 18–20 (2002)

[76] Iwamoto, M., Omori, K., Kimpara, H., Nakahira, Y., Tamura, A., Watanabe, I., Miki, K., Hasegawa, J., Oshita, F., Nagakute, A.: Recent advances in thums:

development of individual internal organs, brain, small female and pedestrian model. In: Proceedings of 4th European LS Dyna Users Conference, pp. 1–10 (2003)

[77] Fang, H., Solanki, K., Horstemeyer, M.: Numerical simulations of multiple vehicle crashes and multidisciplinary crashworthiness optimization. International Journal of Crashworthiness **10**(2), 161–172 (2005)

[78] Kahane, C.J.: Evaluation of fmvss 214-side impact protection: Dynamic performance requirement; phase 1: Correlation of tti (d) with fatality risk in actual side impact collisions of model year 1981-1993 passenger cars; plan for phase 2: Effect of fmvss 214 and correlation of tti (d) with actual fatality risk in model year 1992-2000 passenger cars. Technical report (1999)

[79] Berthelson, P.R., Ghassemi, P., Wood, J.W., Liu, Y., Al-Graitti, A.J., Jones, M.D., Chowdhury, S., Prabhu, R.K.: Evaluation of occupant neck injury response to varied impact conditions using a finite element-mathematical surrogate modeling approach. International Journal of Crashworthiness, 1–17 (2021)

[80] Berthelson, P., Ghassemi, P., Wood, J., Stubblefield, G., Al-Graitti, A., Jones, M., Horstemeyer, M.F., Chowdhury, S., Prabhu, R.: A finite element–guided mathematical surrogate modeling approach for assessing occupant injury trends across variations in simplified vehicular impact conditions. Medical & Biological Engineering & Computing **59**(5), 1065–1079 (2021)

[81] Chen, W., Simpson, T.W., Allen, J.K., Mistree, F.: Satisfying ranged sets of design requirements using design capability indices as metrics. Engineering Optimization **31**(5), 615–619 (1999)

[82] Choi, H.-J., Austin, R., Allen, J.K., McDowell, D.L., Mistree, F., Benson, D.J.: An approach for robust design of reactive power metal mixtures based on non-deterministic micro-scale shock simulation. Journal of Computer-Aided Materials Design **12**, 57–85 (2005)

[83] Sharma, G., Allen, J.K., Mistree, F.: A method for robust design in a coupled decision environment. Design Science **7**, 23 (2021)